ORIGINAL PAPER

Epoxy matrix composites from waste for manufacturing tools for energy efficient moulding process

Gorka Diez-Barcenilla[1] · Alexandra Allue Salvador[1] · Koldo Gondra Zubieta[1] · Ester Zuza[2]

Abstract

In this research, the viability of adding value to grinding steel swarf (GSS) and sheet moulding compound (SMC) residues through its use in the manufacture of hot-press compression moulds is investigated. The moulds serve for small batch production runs of SMC where cost, easy demoulding of parts and energy consumption are three central issues to resolve. The recovery of steel and SMC waste and its use as a filler in replacement of commercial aluminium and $CaCO_3$ powder, to reduce mould manufacturing costs, forms part of the proposed method. It is also an innovative development that may encourage other methods of waste recovery. The epoxy resin filled with 40 wt% GSS is 8.5% harder and 29.5% cheaper than the epoxy filled with aluminium. In addition, the thermal conductivity and density of the epoxy resin filled with 40 wt% SMC were 30.1% and 9.0%, respectively, lower than its counterpart in $CaCO_3$, which meant that the raw material costs of a 4 m^3 mould manufactured with these novel polymer matrix composites registered a cost saving of € 14,028. Furthermore, the results of the moulding experiments confirmed that the hot-press compression mould manufactured with epoxy filled with 40 wt% GSS and SMC was able to manufacture a small batch of parts with no demoulding issues and its innovative thermal barrier provides a saving of 27% in energy consumption.
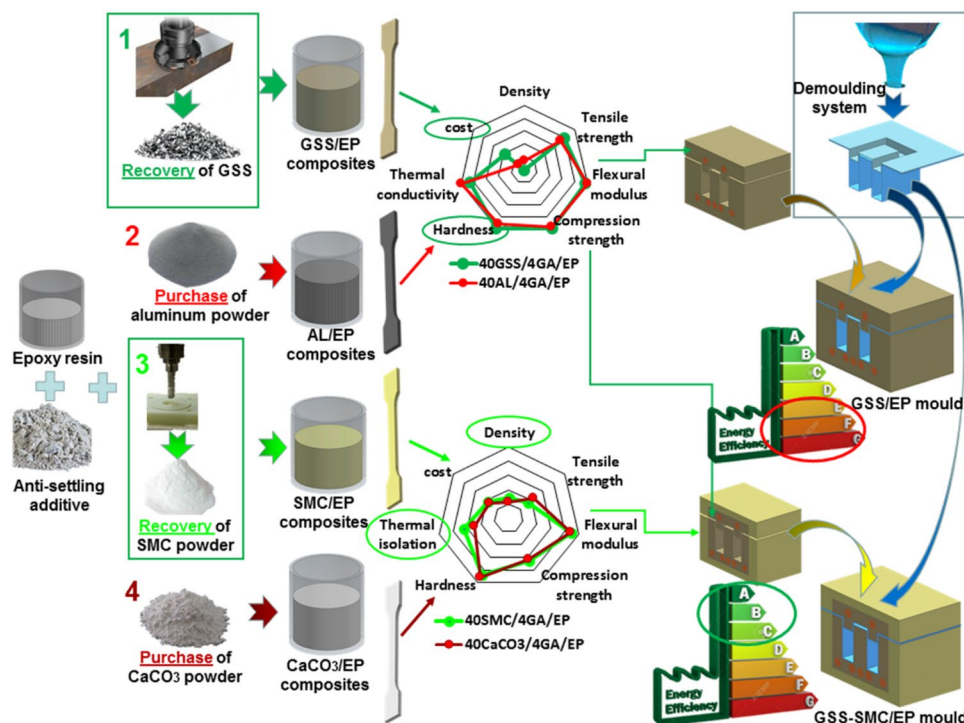
✉ Gorka Diez-Barcenilla
diez@gaiker.es

[1] GAIKER Technology Centre, Basque Research and Technology Alliance (BRTA), Zamudio, Spain

[2] Department of Mining-Metallurgy Engineering and Materials Science, Faculty of Engineering, University of the Basque Country (UPV/EHU), Bilbao, Spain

Graphical abstract

Keywords Waste recovery · Energy efficiency · Rapid tooling · Polymer matrix composites · Compression moulding

Introduction

The future worldwide competitiveness is expected to depend on the energy, a basic resource which is essential for the economic growth (Tuo et al. 2018), where industrial manufacturing electrical consumption contributes with nearly a third of the worldwide consumption (Meng et al. 2019). It is estimated that the energy saving potential of the global manufacturing industry can reach 20% (Gutowski et al. 2013); therefore, in recent years, broad research has been performed in manufacturing processes, using on the one hand energy models (Yan et al. 2016; Winter et al. 2014) and on the other hand optimization algorithms (Salido et al. 2017; Liu et al. 2016; Xu et al. 2016). However, to achieve the ambitious target of minimizing greenhouse gases by 80–95% by 2050 relative to 1990 in Europe (Lechtenböhmer et al. 2016; Sheehan et al. 2016), it is also necessary to promote other strategies, such as material efficiency (e.g. through waste minimization).

In this sense, epoxy resin is presented as a material with a great ability for incorporating waste products (Nóvoa et al. 2004). For instance, Tiwari et al. (2020) and Yin et al. (2020) added fly ash to epoxy to improve some mechanical properties. Likewise, other types of industrial

wastes, such as, cork, polymeric and foundry wastes, have been successfully used as fillers into epoxy and other thermoset matrices (Reis et al. 2013; Ribeiro 2016). Moreover, commercial fillers are also used to enhance some properties of the pristine epoxy (Table 1).

In this paper, two novel and cost-effective PMCs based on epoxy resin filled with two milling wastes (GSS and SMC) are presented.

GSS is a very tiny steel chip obtained from high-speed machining which is complicated to handle in recycling systems (Takagi et al. 2012). In addition, the high running costs and energy demand of the recycling techniques make them economically feasible for recycling metallic swarf with high market prices, such as, aluminium (1600 $/Ton), copper (2100 $/Ton), brass (1500 $/Ton) and stainless steel (640$/Ton), whereas cast iron and steel swarf (20 $/Ton and 90 $/Ton, respectively) are less attractive to recycle (da Costa et al. 2003). To manage this waste (e.g. 10 tons of GSS are discharged in a bearing factory every day) (Nakamura 2004), Shukla (2013) and Seetharam et al (2017) reused this waste adding to concrete at different wt%. Takagi et al. (2012) valorized the GSS by making a disposable body warmer instead of using commercial iron powder.

Table 1 Filler additions and their effects on epoxy resin properties

Property	Research	References
Thermal	Influence of the addition of fillers on the thermal conductivity of epoxy resins	(Kuo and Li 2017; Khushairi et al. 2017; Fu et al. 2010; Tomori et al. 2004)
Thermal	Influence of the addition of fillers on the linear expansion of an epoxy resin	(Ma et al. 2007)
Mechanical	Influence of the addition of fillers on the compressive properties of epoxy resins	(Ma et al. 2007; Khushairi et al. 2015; Bhagyashekar and Rao 2010; Gope 2011)
Mechanical	Influence of the addition of fillers on the tensile and flexural properties of epoxy resins	(Khushairi et al. 2015; Bhagyashekar and Rao 2010)
Mechanical	Influence of the addition of fillers on the impact properties of epoxy resins	(Kuo and Li 2017; Burmistrov et al. 2014; Mostovoi et al. 2017)
Physical	Influence of the addition of fillers on the hardness of epoxy resins	(Khushairi et al. 2017, 2015; Ma et al. 2007; Chung et al. 2005; Bhagyashekar et al. 2009)
Physical	Influence of the addition of fillers on the density of epoxy resins	(Khushairi et al. 2017; Bhagyashekar et al. 2009)
Physical	Influence of the addition of fillers on the wear resistance of epoxy resins	(Kuo and Li 2017; Khushairi et al. 2017, 2015; Ma et al. 2007; Vasconcelos et al. 2006)

SMC powder is another common waste in machining factories due to the rise of the manufacture of glass fibre reinforced plastics (GFRPs) which achieved 1069 million tonnes in 2015 (Jensen and Skelton 2018). Consequently, high quantities of scraps and post-production machining waste (estimated to account for between 5 and 40% of total GFRPs production volume) (Shuaib and Mativenga 2016) were traditionally managed by controlled disposal or incineration (Garcia et al. 2014). However, recent stricter legislations have limited the amount of organic material allowed to be landfilled or incinerated. Thus, nowadays landfill is highlighted as the least preferred option according to the waste hierarchy, where mechanical recycling is the preferred one (Shuaib and Mativenga 2016). Mechanically recycled GFRP waste has been incorporated in many products, such as SMCs and bulk moulding compounds, concrete, polymer concrete and so on (Ribeiro et al. 2016, 2011). However, sometimes this recyclate does not affect positively to some properties of the PMC, or the costs of the mechanical recycling exceed the market value of the competitor virgin product, the calcium carbonate, which is one of the barriers identified (Ribeiro et al. 2013).

In this article, the developed PMCs are used to manufacture a cost-effective compression mould for small batch production runs of SMC that is also energy efficient. The traditional steel mould manufacturing method is neither cost-effective for small batch production nor sustainable, because it consumes a considerable amount of electricity and generates a lot of metal chip waste (de Carvalho et al. 2016; Bernard and Fischer 2002).

To solve the issue of waste generation, an alternative approach has been developed using selective laser melting (SLM) (Fettea et al. 2015; Mahshid et al. 2016). However, the largest SLM printer to date has a maximum printing area of $0.4m^2$ (according to Hollaway (1994), part sizes for SMC moulding ranges from 0.1 to $3m^2$) and the cost of the metals used and the SLM average printing speed amounts to hundreds of Euros per kilo and $150cm^3/h$ (Khorasani et al. 2020), respectively. In an effort to reduce material usage and to speed up part production, several studies on the use of lattices structures (Pan et al. 2020; Flores et al. 2020) have obtained 60% reductions in the load-bearing capacity and savings in raw materials of 30%. Even so, it is still a time-consuming process that produces relatively small and expensive SMC compression moulds with costly equipment that is not free from some part demoulding difficulties (Pontes et al. 2010; Goncalves et al. 2007).

Experimental procedure

Materials

Uneresin 3710 AF (6500–8000 mPa s) epoxy resin and Unedur 3711 AF (30–50 mPa s) hardener (Uneco S.A.) were selected as the resin and hardener system. A powdered rheology additive Garamite-7305 (BYK-Chemie GmbH) was used for an increase in viscosity within the low shear range.

The machining factory Composites Martiartu S.L. supplied the SMC and GSS wastes. SMC powder was obtained from SMC parts milling. This polyester SMC (Verkid PG18-G250 1015; Astar S.A.) has a surface mass of $4.500 \ gr/m^2$, and a glass fibre content of 18wt% (chopped strand mat). The GSS (alloyed steel) was collected from a band saw.

The aluminium powder was purchased from Feroca S.A. and the $CaCO_3$ powder was supplied by Jesus Suministros S.A. The specific density of these materials and the particle size distribution of the fillers are shown in Table 2.

Table 2 Materials granulometry and specific density

Material	Particle size				Specific density (gr/cm³)
	800 μm (wt%)	150 μm (wt%)	100 μm (wt%)	40 μm (wt%)	
Uneresin 3710AF	–	–	–	–	1.17
Unedur 3711AF	–	–	–	–	0.92
GSS	81	49	29	16	7.85
Al	100	99	89	35	2.70
SMC	100	98	92	46	1.82
CaCO₃	–	–	100	99	2.71

Characterization of fillers

Scanning electron microscopy–energy-dispersive X-ray spectroscopy (SEM–EDX) analysis was performed, to confirm the nature and the morphology of the GSS and SMC. A morphology analysis was also performed to aluminium and $CaCO_3$ fillers. A TGA (STAR SW; Mettler Toledo, Inc.) was performed, to ensure the removal of the cutting fluid from the GSS, which was previously sieved with a 100 microns mesh. The GSS sample was heated up to 600 °C from 25°C at a rate of 10 °C min^{-1} in a nitrogen atmosphere. Prior to its analysis in the SEM–EDX (model EVO 50; ZEISS A.G.), all samples were metallized with a layer of Au and Pd (80 and 20 wt%, respectively) with a thickness of approximately 5 nm. The observations were performed in high vacuum with a voltage of 20 kV. The equipment has a secondary electron (SE) detector and a backscattered electron detector (BSD) which gives compositional information on the sample.

PMC test sample manufacturing

The fillers were introduced into a convection oven (AFA 200/768; Dycometal S.L.), for 1 h at 105 °C to remove any moisture. Previously the GSS were sieved with a 100 μm mesh. The PMC manufacturing process was as follows: 1134.0 g epoxy resin and 306.2 g hardener were mixed with a stirrer (SL-1; Lleal Process S.A.U.) at 120 rpm for 5 min. Then, 60.0 g of Garamite was added to the catalysed resin, mixed with the stirrer at 120 rpm for 3 min and poured into five containers. Subsequently, four PMCs (and a fifth blend with no filler) were obtained by pouring four different proportions of filler (10%, 20%, 30% and 40%) by weight into the catalysed resin (as shown in Table 3). The

Table 3 Constituents of the PMCs

Specimen ID	Epoxy (EP) content (wt%)	Hardener content (wt%)	Garamite (GA) content (wt%)	Filler type	Filler content (wt%)
EP	78.75	21.26	–	–	–
10GSS/4GA/EP	68.03	18.37	3.60	GSS	10.00
20GSS/4GA/EP	60.47	16.33	3.20	GSS	20.00
30GSS/4GA/EP	52.91	14.29	2.80	GSS	30.00
40GSS/4GA/EP	45.4	12.25	2.40	GSS	40.00
10AL/4GA/EP	68.03	18.37	3.60	AL	10.00
20AL/4GA/EP	60.47	16.33	3.20	AL	20.00
30AL/4GA/EP	52.91	14.29	2.80	AL	30.00
40AL/4GA/EP	45.40	12.25	2.40	AL	40.00
10SMC/4GA/EP	68.03	18.37	3.60	SMC	10.00
20SMC/4GA/EP	60.47	16.33	3.20	SMC	20.00
30SMC/4GA/EP	52.91	14.29	2.80	SMC	30.00
40SMC/4GA/EP	45.40	12.25	2.40	SMC	40.00
10CaCO₃/4GA/EP	68.03	18.37	3.60	CaCO₃	10.00
20CaCO₃/4GA/EP	60.47	16.33	3.20	CaCO₃	20.00
30CaCO₃/4GA/EP	52.91	14.29	2.80	CaCO₃	30.00
40CaCO₃/4GA/EP	45.40	12.25	2.40	CaCO₃	40.00
10GSS/2GA/EP	69.45	18.75	1.80	GSS	10.00

same methodology was performed to manufacture the aluminium, SMC and $CaCO_3$ filled composites. Each blend was manually mixed with a stirrer for 5 min, introduced into the vacuum chamber for 20 min (just for GSS and aluminium blends) and cast in fifteen rectangular wooden moulds (waxed with MouldWiz mould release paste wax supplied by Axel ApS) and five silicone rubber moulds (Xiameter RTV-4136-M; Dow Corp.) with cylindrical shapes. The moulds were introduced into the convection oven at 40 °C with an increase in temperature of 20ºC/h until reaching an oven temperature of 160 °C that was maintained for 1 h. Finally, the temperature was lowered at 20 °C/h until reaching room temperature and the samples were demoulded.

Test specimens conforming to type II (ASTM D 638), $12.7 \times 12.7 \times 25.4$ mm (ASTM D 695), $127 \times 12.7 \times 3.5$ mm (ASTM D 790), $20 \times 20 \times 3.5$ mm (ISO 1183–1) and $200 \times 150 \times 4$ mm (ASTM D 2583) were used for tensile, compressive, flexural, density and hardness tests, respectively. Tensile test dumbbell specimens were machined with a CNC (C-3C; Graphimet S.A.). The other specimens were cut with a circular saw (49,716 meppen; Metabo, S.A.). Cylindrical samples of 6 mm in diameter by 30 mm were manufactured with silicone rubber moulds. Samples of 1.0–1.5 mm in thickness were then extracted using a precision saw (Isomet; Tecnomet S.L.) to perform thermal conductivity tests.

Sedimentation analysis of GSS PMCs

For sedimentation analysis, two $5 \times 10 \times 3$ mm samples were manufactured: 10GSS/4GA/EP and 10GSS/2GA/EP. SEM analysis revealed the distribution of the GSS filler (without being sieved) within the epoxy matrix.

Thermal characterization of PMCs

Filings were extracted from 40GSS/4GA/EP and 40AL/4GA/EP and introduced into differential scanning calorimetry (DSC) equipment (DSC1; Mettler Toledo Inc.), to obtain the Tg. Samples were heated up to 250 °C from -50 °C at a rate of 10 °C min^{-1} in a nitrogen atmosphere. The Tg was calculated from the first heating scan. Three slopes and two points of intersection were obtained. The midpoint between these two intersection points was taken as the Tg value.

DSC analysis was performed to obtain the thermal conductivity. The method consisted of placing gallium on the upper circular end surface of the sample. The temperature difference and heat flow between the upper and lower end surfaces of the disc were measured. The thermal conductivity (λ=W/m K) was calculated with Eq. (1) (Thermal Analysis Application 2010):

$$\lambda - \phi/\Delta T + h/A \tag{1}$$

where ϕ represents the heat flow (W), ΔT the temperature difference (K), h the thickness of the sample (mm) and A the cross-sectional area (mm^2). Two samples of each composition were tested, and the average value and the standard deviation were reported.

Two TGA were performed to evaluate the thermal stability of the 40GSS/4GA/EP and the Garamite-7305. The samples were heated up to 600 °C from 25 °C at a rate of 20 °C min^{-1} in a nitrogen atmosphere.

Mechanical characterization of PMCs

Test specimens were conditioned in a standard 23/50 case 2 atmosphere (ISO 291). A universal electromechanical test frame (AGS-X 100KN; Shimadzu, Inc) with a 5KN load cell was used to perform the tests. For flexural and tensile modulus measurements, a video extensometer (DVE-201; Sony, Inc.) with an accuracy of 1% and a contact extensometer (MFA2; Techlab Systems, S.L.) with an accuracy of 0.2%, respectively, were used. Tensile test specimens were fixed with wedge grips and loaded with a crosshead speed of 5 mm/min. Flexural test specimens were tested with a support span of 16 times the thickness of the beam and loaded with a strain rate of 0.01 mm/mm/min (A method). Compression test specimens were placed between two metallic compression plates. They were compressed with a crosshead speed of 1.5 mm/min. Five samples for each composition were tested, and the average value and the standard deviation were reported.

Physical characterization of PMCs

Test specimens for hardness tests were conditioned in accordance with method A of Practice D618. 29 readings were performed (with Model No. 935 the Barcol Impressor), needed for non-homogeneous materials and for the lowest Barcol level. An analytical balance (Mettler AE260 Delta Range; Mettler Toledo Inc) was used with density tests. An immersion method was used with isopropyl alcohol as the immersion liquid. Three samples for each composition were tested. The equations of the theoretical densities of the composites were obtained by rule of mixture (Bhagyashekar et al. 2009): Eq. (2). Microsoft excel was used to obtain the trend curves and the 2nd order polynomial function was the one which best suited the theoretical results. The void percentage was calculated by Eq. (3), where d represents density, V represents volume fraction, and the terms in subscript $_{v, C, f, m}$ and $_{Ctest}$ represent the voids, the composite, the filler, the matrix and the tested composite (Nayak et al. 2020). Furthermore, SEM observations of 40GSS/4GA/EP, 40AL/4GA/EP, 40GSS/4GA/EP and 40CaCO$_3$/4GA/

EP were performed to identify the presence of voids. Test samples were cut with the precision saw and the surfaces were metallized with a layer of Au and Pd (80 and 20 wt%, respectively) with a thickness of approximately 5 nm. The observations were performed in high vacuum with a voltage of 20 kV.

$$d_c = d_m v_m + d_f v_f \qquad (2)$$

$$V_v = \left(d_c - d_{\text{Ctest}}\right)/d_c \qquad (3)$$

Cost analysis and PMC selection

The cost per kilogram was calculated for each PMC, considering the weight fraction of each constituent (Table 3) and its cost (resin system: €10.3/kg, aluminium: €6.5/kg, $CaCO_3$: € 0.7/kg, GSS and SMC: €0/kg. The contribution of the Garamite to the overall cost was disregarded, due to the small amount added to the blend and its price (€12.1/kg). The information on costs was used to calculate the raw material cost of building two types of moulds: Al/EP mould and GSS/EP—SMC/EP mould (Fig. 1), considering that SMC/EP occupies the 55% of the total mould volume. Furthermore, four mould sizes were analysed: small $5 \times 5 \times 2.5$ dm^3; medium, $10 \times 10 \times 5$ dm^3; large, $15 \times 15 \times 7.5$ dm^3; and very large $20 \times 20 \times 10$ dm^3.

The method to select the most suitable PMC uses the results of the obtained properties (San-Jose et al. 2015). The maximum value is designated the unit, and the remaining relative indices are calculated by dividing the value to be analysed by the maximum value. Relative indices were multiplied by a weighting factor (ranging from 1 to 5: where 1 is unimportant and 5, extremely important), and finally, they were all added or subtracted, depending on whether the property was to be maximized or minimized. The highest value represented the most interesting material and the lowest value, the least interesting for mould manufacturing.
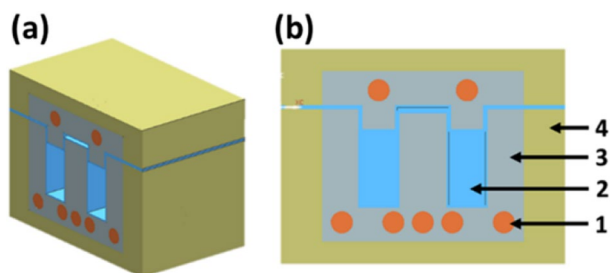
Fig. 1 Mould design of $23 \times 19 \times 13$ cm (W $\times$ D $\times$ H). (**a**) GSS/EP-SMC/EP mould cross section in an isometric view. (**b**) GSS/EP-SMC/EP mould cross section in a front view: 1: copper ducts, 2: silicone covers, 3: 40GSS/4GA/EP, 4: 40SMC/4GA/EP

Mould design, manufacturing and testing

Figure 1 mould (designed with Siemens NX10 software) is divided into an internal thermally conductive volume and an external thermal barrier. To ease the demoulding of parts, two silicone covers of 4 mm thick were designed with 1.5 mm clearance between them for a positive mould closure type.

The construction scheme of Fig. 1 mould and another mould made entirely of 40GSS/4GA/EP are shown in Fig. 2. Both the master model and the mould frame of these moulds were manufactured with a fused deposition modelling (FDM) printer (3NTR-A2; 3NTR srl) using white standard and leaf/green PLA/PHA filament (Colorfabb B.V.). Demoulded moulds were post-cured in the convection oven for 13 h (6 h of heating from 40 to 160 °C with an increase in temperature of 20 °C/h and 7 h of cooling with a decrease in temperature of 20 °C/h).

Each mould was placed between two fibre–cement plates of 1 cm thick and then located between two steel plates of the universal testing machine. An oil heating machine (STO 109; Diapam S.A.) was connected to the mould and programmed (in two steps) to heat the oil to 120 °C. When a steady state was reached, it was begun to introduce each SMC stack-up (Verkid PG18-G250 1015) into the female mould at all time intervals in which the oil heating machine was switched off for the next seven hours. Each stack-up was weighed, introduced on approximately the 80% of the moulding surface and compressed at different test speeds. Although a cure time of 27 ± 5 s/mm of thickness at 140 °C is recommended, the moulding time has been increased to 90 s/mm, to counteract the lower moulding temperature (Barone and Caulk 1979). To prevent any possibility of moulded part marking, no decompression procedure was performed.

Thermocouples were located at two positions (Fig. 3) and connected to a data logging software (PicoLog 6; Pico technology, Ltd) for real-time temperature monitoring. The thermocouple located at the oil inlet notices the moments when the oil heater switches on and off; thus, knowing the machine's operating time and its power (7.5KW), the energy consumption during the steady-state period is calculated.

Results and discussion

Characterization of fillers

The aluminium particles show an ellipsoidal and spherical shape with some protuberances on the surface, whereas $CaCO_3$ particles show an irregular shape and with a size that ranges approximately from 1 to 40 microns.

Curve-shaped swarfs of various sizes are observed in Fig. 4. The EDX spectrums of four swarfs identify same

Fig. 2 Construction scheme of male moulds. (**a**) Construction of a 4-mm-thick silicone rubber cover in two steps (curing of 2 h at 45 °C in a convection oven after each step): 1) bottom flat base: by pouring the silicone rubber into the 3D printing master model; 2) vertical walls and top flat surface: by pouring the silicone rubber into the master model and two auxiliary 3D printing mould frames. (**b**) Placement of the copper heating channels. (**c**) Pouring of the 40GSS/4GA/EP. Demoulding after 6 h curing at ambient T° (20 °C). (**d**) Pouring of the silicone rubber. Curing of 2 h at 45 °C. (**e**) Pouring of the 40SMC/4GA/EP. Demoulding after 6 h curing at ambient T° (20 °C)
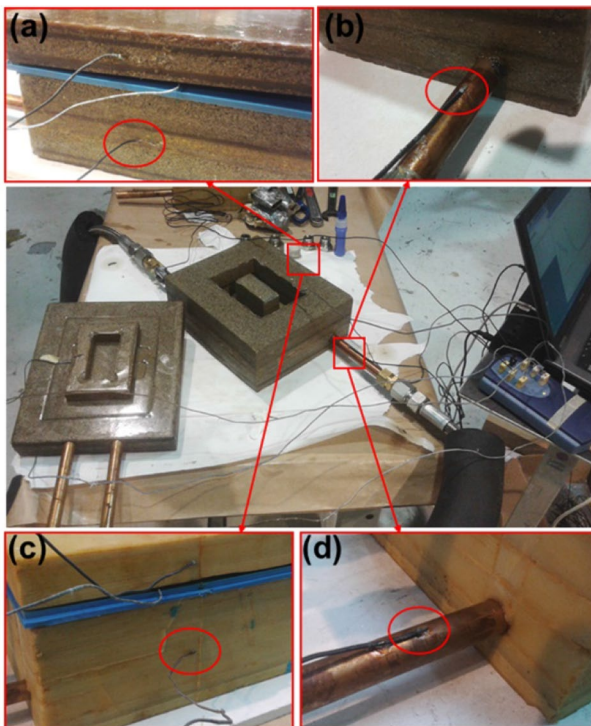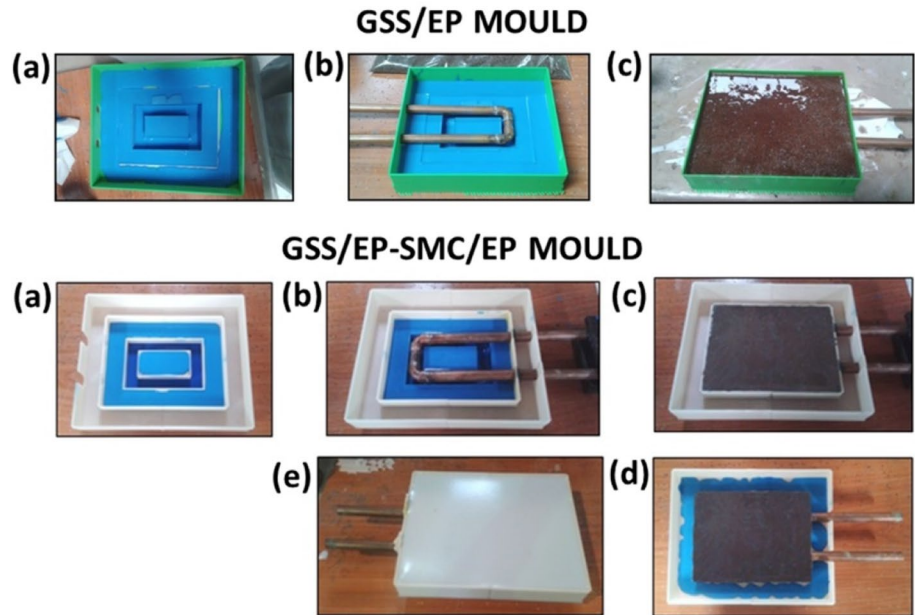
Fig. 3 Thermocouple locations in the moulds. GSS/EP mould: (**a**) mould wall and (**b**) oil inlet. GSS/EP—SMC/EP mould: (**c**) mould wall and (**d**) oil inlet

chemical elements—Fe, Mn, Si and Co—in all spectrums with the following average wt% (and standard deviation): 96.43% (0.33%), 1.62% (0.06%), 0.53% (0.09%) and 0.65% (0.07%), respectively. As stated in EN 10,020, an alloyed steel contains a higher content of the elements listed in EN 10,020 (Table 1) than the limit value shown in the aforementioned table. In this case, cobalt exceeded that limit value (0.65 wt% > 0.30 wt%) which confirmed that the four swarfs under analysis are identified as alloyed steel, because neither chromium (found in stainless steel) was present, nor cobalt is commonly found in cast iron.

Figure 4 also shows SMC powder which consists of particles of different sizes and shapes and some fibres. These particles are identified as resin and $CaCO_3$ particles according to the EDX (b2), (b4) spectrums, respectively. (b2) spectrum show a wt% of 47.57% and 37.89% of carbon and oxygen, as well as aluminium (6.36%) which indicates that an organic compound predominates and that there are traces of some additive, for instance, alumina, used to improve the electric arc resistance of the SMC (Lokensgard 2010). The presence of $CaCO_3$ is confirmed by the (b4) spectrum, which shows a wt% of 17.92%, 47.33% and 33.77% of carbon, oxygen and calcium (according to Davis (2003), and an SMC standard formulation can contain up to 40% calcium carbonate). The high percentages of Si and O showed in the spectrum (b1) confirm the nature of the fibres. (b3) spectrum analysis area gathers different particles and a fibre.

Sedimentation analysis of GSS PMCs

Figure 5 shows the sedimentation observations (in cross section) of the non-sieved GSS filler for 10GSS/4GA/EP and 10GSS/2GA/EP, where an improvement in filler dispersion and reduced amounts of agglomerates can be observed with the increase in Garamite-7305 content. 10GSS/4GA/EP showed quite a homogeneous GSS filler dispersion with no relevant agglomerates in the host matrix, whereas 10GSS/2GA/
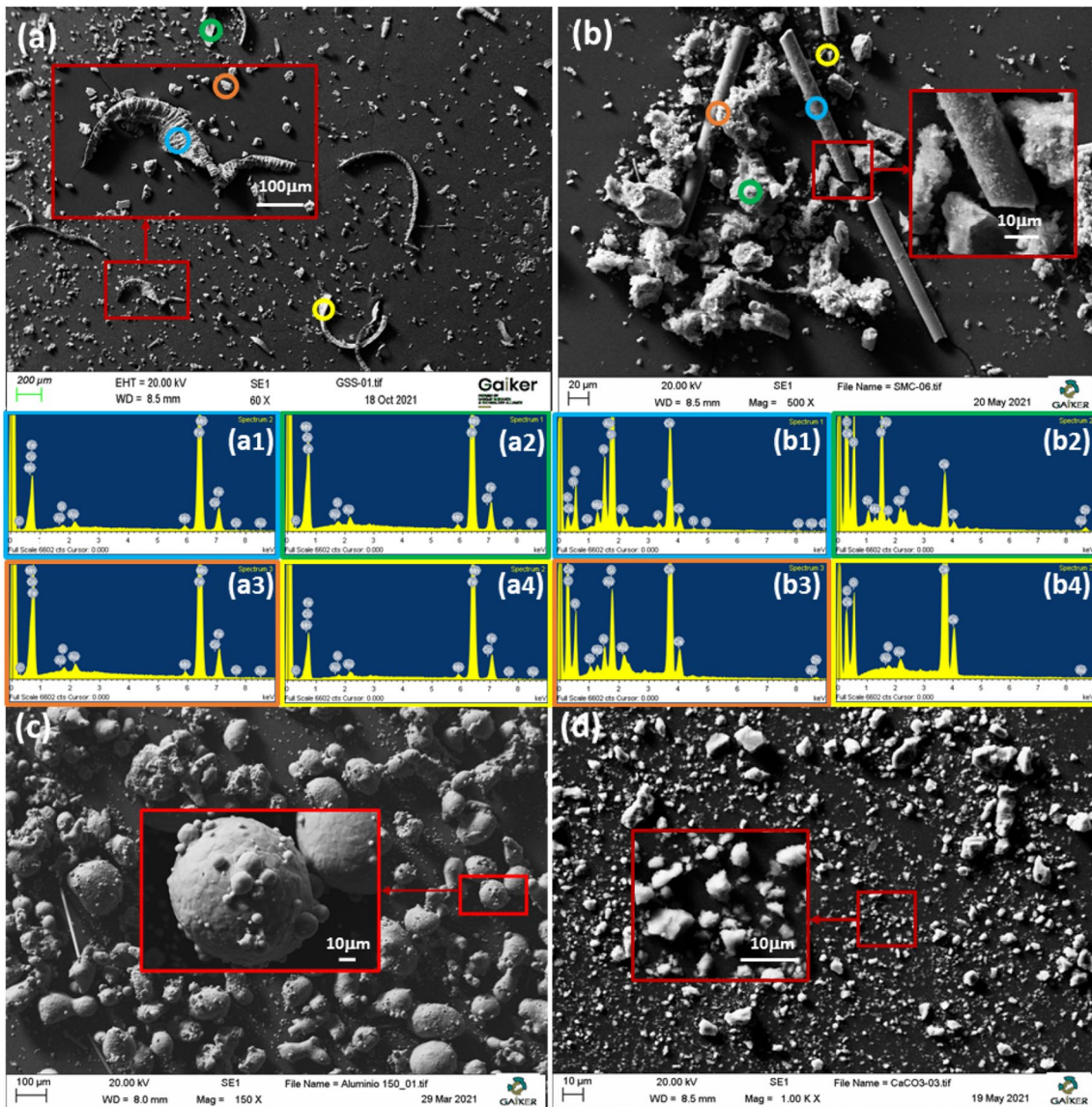
Fig. 4 SEM micrographs of GSS (**a**), SMC (**b**), Al (**c**) and CaCO$_3$ (**d**) at different magnifications. EDX spectrums of four GSS (a1), (a2), (a3), (a4) and four SMC (b1), (b2), (b3), (b4) randomly selected particles
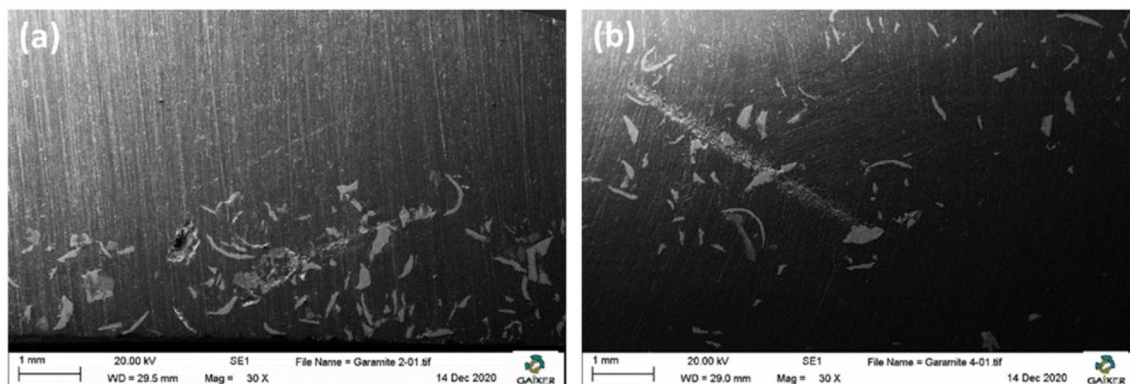
Fig. 5 SEM micrographs for the filler dispersion analysis. (**a**) 10GSS/2GA/EP. (**b**) 10GSS/4GA/EP

EP showed GSS particle dispersion with large agglomerates because the resin did not reach a sufficient viscosity.

In view of the results, it is necessary to add this powdered thixotropic agent in quantities of at least 4wt%, in order to increase the viscosity of the epoxy resin sufficiently in the low shear range and to reduce the GSS sedimentation velocity drastically.

Other anti-settling proposals such as employing higher quantities of accelerators or temperature to accelerate the curing process of the matrix, even used in conjunction with specially designed anti-sedimentation devices, were also studied (Leite et al. 2013). However, the novel approach shown in this article has the advantage that there is no need for a comprehensive resin curing study to define the manufacturing strategy nor there is a need to manufacture a specific anti-sedimentation device.

Thermal characterization of PMCs

As summarized in Table 4, the pristine epoxy showed the highest Tg value, whereas 40GSS/4GA/EP showed the lowest Tg. The degree of cross-linking of these compounds was therefore relatively similar. This difference is probably due to a slight residual moisture still present in the aluminium and the GSS fillers together with a possible reaction of the epoxy resin with iron oxide in the case of the 40GSS/4GA/EP.

Thermally conductive PMCs embed the copper ducts; therefore, the composite must achieve a higher Tg than 120ºC (oil temperature) to avoid a sudden weakening of its mechanical properties, which could lead to mould breakage.

Figure 6 shows the thermal conductivity of the pristine epoxy and the corresponding PMCs filled with GSS, aluminium, SMC and $CaCO_3$ up to 40wt%. 40AL/4GA/EP showed the highest thermal conductivity value, 0.50 ± 0.11 W(mk)$^{-1}$, among them all, whereas the second highest value, 0.43 ± 0.09 W(mk)$^{-1}$, corresponded to 40GSS/4GA/EP. These results were consistent with the literature where the thermal conductivity of the PMCs is influenced by the thermal conduction capacity of the filler and the filler content (Callister 1999; Chiu et al. 2015).

High thermal conductivity is desirable when moulds undergo thermal cycling, because the temperature gradient on the moulding surfaces is minimized, producing better pieces in terms of dimensional stability. Furthermore, this temperature variance issue is amplified when thin parts are moulded (Barone and Caulk 1980). On the contrary, low thermal

conductivity materials are preferred when a mould needs to be thermally insulated, so that the energy loss to the environment is reduced.

In this sense, both polyester resin and fibreglass (the main compounds of the SMC) and epoxy resin, have lower thermal conductivity than $CaCO_3$ (Yusof et al. 2018). This is consistent with what is shown in Fig. 6, where $CaCO_3$/EP PMCs exhibit an increase in their thermal conductivity with $CaCO_3$ content. However, the slope of the obtained trend curve is lower than what is shown in the literature (Vakili et al. 2011; Yusof et al. 2018). Having a high number of voids (according to Osugi et al. (2009) thermal conductivity of the air is 0.026 W/mk) in the PMC may be the reason why the increase is smoother. On the contrary, the thermal conductivities of SMC/EP PMCs are almost unaffected with SMC addition, which could indicate that there is not a very high percentage of calcium carbonate in the SMC as it might think. Moreover, the glass fibre helps to counteract the presence of $CaCO_3$, because it possesses lower thermal conductivity (0.04 W/mk, according to Modarresifar et al. (2016)) compared with the remaining materials.

Figure 7 shows the thermal stability of 40GSS/4GA/EP and Garamite-7305. 40GSS/4GA/EP began to lose its thermal stability after approximately 300ºC (quite far from the operating temperature of the mould) and showed a loss on ignition of 48,4%. On the contrary, the Garamite showed a loss on ignition of 24,7% (which meant 1% of the introduced 40GSS/4GA/EP sample). Furthermore, the epoxy resin partially carbonizes under nitrogen atmosphere due to its aromatic rings from bisphenol A, which would explain the difference between the obtained loss on ignition (48,4%) and the expected value (57%).

Mechanical characterization of PMCs

High compression strength is a desirable property, due to the requirements for clamping force in high-pressure moulding processes (Khushairi et al. 2015). Tensile and flexural properties are the parameters that affect the mould wall sizing and other structural details of the moulds.

Figure 6 shows the tensile strength reduction with the filler content in agreement with the literature (Khushairi et al. 2015; Bhagyashekar and Rao 2010). Defects such as cracks and fillers, control the tensile properties of the PMC and these can act as a source of stress that causes structural weakness by introducing discontinuities in the stress transfer process across the filler–resin interface. Thus, it is expected that the filler and voids volume fraction, the interface adhesion between filler and matrix, the extent of the load sharing mechanism and the strength of the filler will quantitatively determine the tensile strength of the compound. In the case of SMC/EP and $CaCO_3$/EP composites, the high number of discontinuities due to their raised voids and filler volume

Table 4 Tg of the PMCs and the pristine epoxy

Specimen ID	Tg (ºC)
EP	152.3
40GSS/4GA/EP	147.4
40AL/4GA/EP	149.4
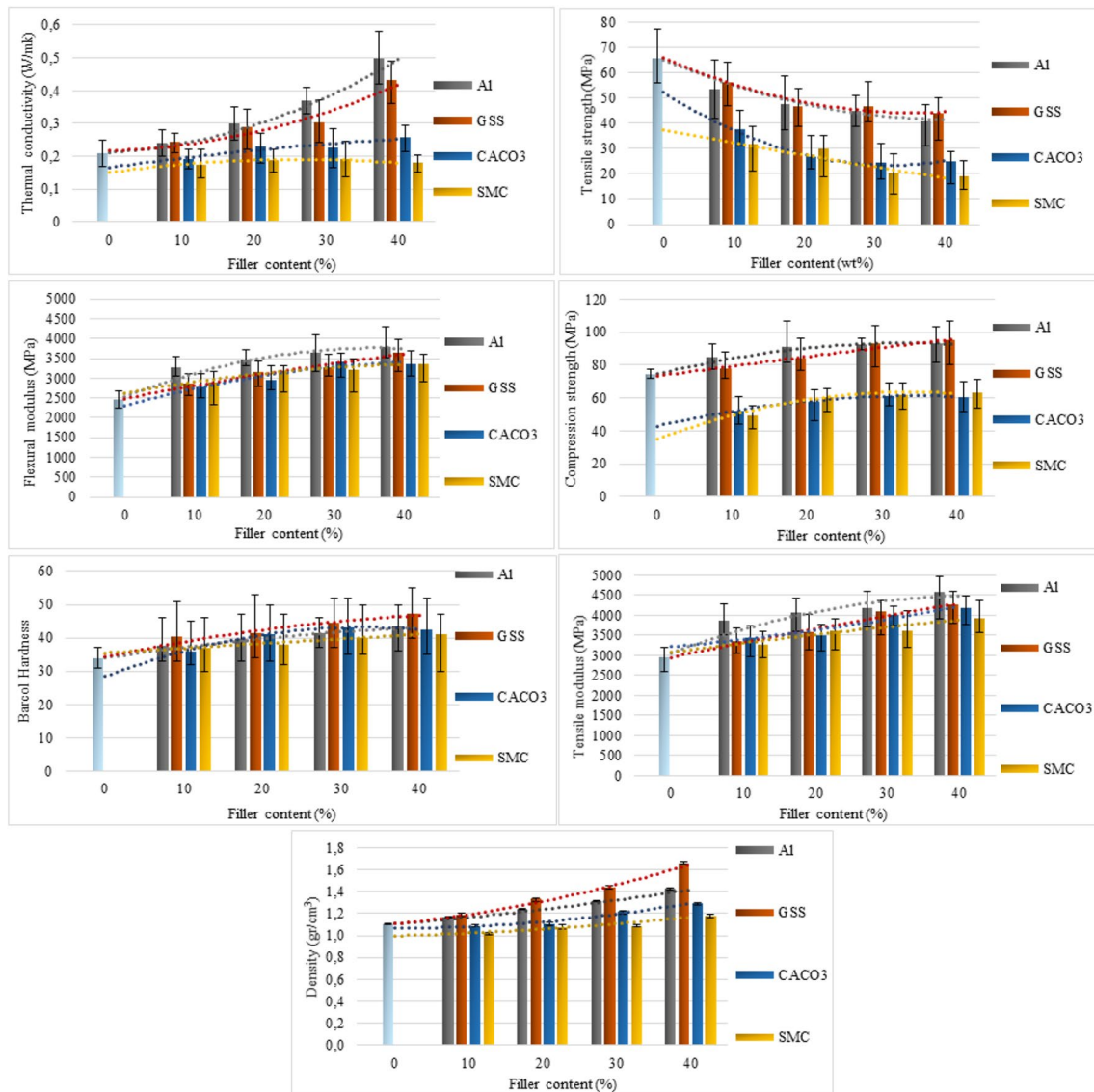
Fig. 6 Thermal, mechanical and physical properties of GSS/EP, AL/EP, SMC/EP and CaCO$_3$/EP PMCs with different filler content

fraction seems to be the reason for the lower tensile strength of these composites compared with GSS/EP, AL/EP and the aforementioned literature. On the contrary, GSS composites, which enclose the lowest filler volume fraction show the greatest tensile strength.

Figure 6 shows the increase in the flexural modulus with the filler content that agreed with the literature (Bhagyashekar and Rao 2010), where 40AL/4GA/EP showed the maximum flexural modulus (3.800 ± 233 MPa). When the AL/EP trend curve reached 40 wt% (22 vol%) of the filler content, a maximum in the mathematical function appears to have been achieved. This trend was not observed for the GSS/EP curve, probably because the GSS volume fraction in its corresponding wt% was lower than that of aluminium (9 vol% in the case of 40 wt%). Likewise, CaCO$_3$/EP

trend curve achieved the maximum at 30wt% filler content (21 vol%), whereas SMC/EP composites hardly increased their flexural modulus beyond 20wt% filler content. These behaviours were in accordance with the rule of mixtures (Callister 1999) where the modulus of the composite will tend to increase with the filler volume fraction and with the elastic modulus of the filler. However, when the added filler exceeds a certain volume fraction, apparently the elastic modulus is negatively affected. As it happens with flexural modulus, the tensile modulus (Fig. 6) also increases with the filler content and the elastic modulus of the filler, which is consistent with the literature (Bhagyashekar and Rao 2010; Callister 1999). Therefore, despite the raised elastic modulus of the GSS, 40AL/4GA/EP showed the highest tensile modulus due to its elevated filler volume fraction.
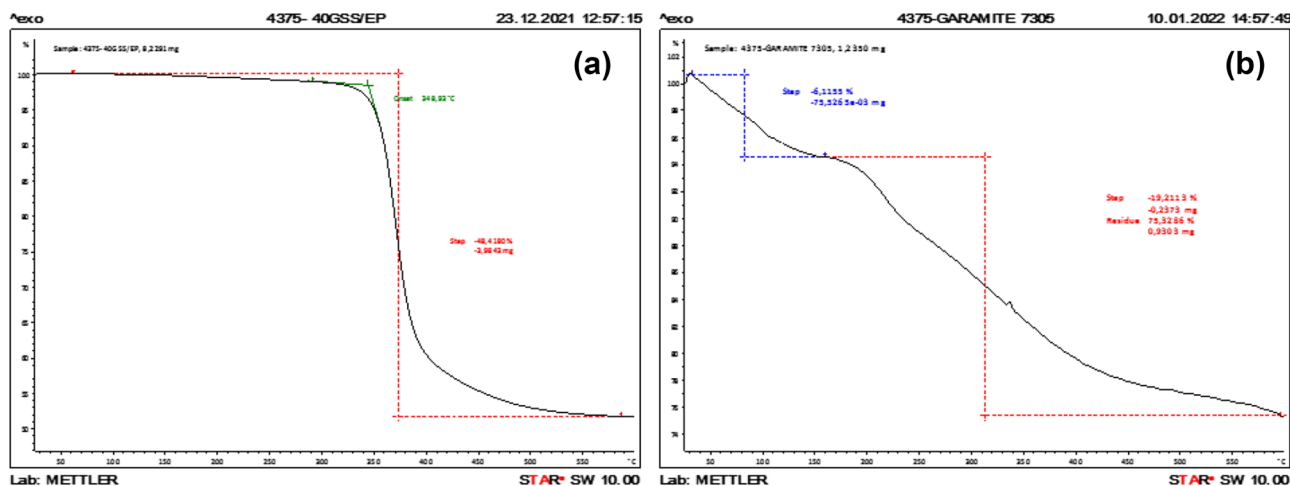
Fig. 7 TGA of 40GSS/4GA/EP (**a**) and Garamite-7305 (**b**)

Figure 6 also shows the increase in the compressive strength with the filler content, since these aggregates contribute to the load-bearing capacity of the composite, rather than acting as a stress source as occurs in a tensile stress state. So, defects caused by the filler tend to close, contrary to the crack opening mechanism that occurs under tensile loading. However, all composites hardly increased their compressive strength beyond 20wt%-30wt% filler content, these behaviours having previously been reported in the literature (Ma et al. 2007; Bhagyashekar and Rao 2010) where nearly all PMCs showed the highest strength prior to 40wt%. The difference in the filler volume fraction between aluminium, GSS, SMC and $CaCO_3$ composites and a possible saturation of filler (i.e. defects) in the test sample cross section, could lead to decrease the load-bearing capacity of the composite; so, this may be the reason why aluminium, SMC and $CaCO_3$ PMCs nearly reached the maximum compressive strength at a lower wt% than GSS PMCs. Furthermore, the high void volume fraction of SMC and $CaCO_3$ PMCs seems to be the reason for the lower compression strength of these composites compared with GSS/EP, AL/EP and the literature (Khushairi et al. 2015; Bhagyashekar and Rao 2010).

Physical characterization of PMCs

The hardness of epoxy-based composites is a key parameter that affects durability and mould life (Ma et al. 2007) because hardness is related to wear resistance (Khushairi et al. 2017). Figure 6 presents the Barcol hardness of the PMCs where 40GSS/4GA/EP (47 ± 4) showed the highest value, confirming that hardness increases with the filler content and with the hardness of the filler (Bhagyashekar et al. 2009).

The mould weight and its manageability are determined by the material density. So, according to Fig. 6, a mould manufactured with 40GSS/4GA/EP and 10SMC/4GA/EP will be the heaviest and the slightest mould, respectively, considering that density increases with the addition of fillers and the density of the filler (Bhagyashekar et al. 2009). Equations (4), (5), (6) and (7) of the predicted values trend curves are shown below:

$$D_{GSS} = 2.0E^{-4}x^2 + 0.0083x + 1.11 \tag{4}$$

$$D_{AL} = 6.0E - 5x^2 + 0.0062x + 1.11 \tag{5}$$

$$D_{SMC} = 6.0E^{-5}x^2 + 0.0018x + 1.00 \tag{6}$$

$$D_{CaCO3} = 6.3E^{-5}x^2 + 0.0050x + 1.00 \tag{7}$$

The predicted values of Eqs. (4), (5) and the experimental data have quite a good correspondence. Therefore, these outcomes corroborated a good GSS and Al particle distribution and the presence of a low percentage of voids (volume fraction < 3.7% in these PMCs) throughout the matrix. On the contrary, if Eqs. (6) and (7) are compared with the experimental data, a considerable difference is observed, due to their relatively high percentage of voids (up to 13,6%) because no vacuum has been applied to them.

These statements are in accordance with SEM observations (Fig. 8) because 40GSS/4GA/EP and 40AL/4GA/EP show fewer and smaller voids than 40CaCO$_3$/4GA/EP and 40SMC/4GA/EP. Furthermore, these SEM micrographs showed a homogeneous filler dispersion (with no significant agglomerates) in the epoxy matrix except 40SMC/4GA/EP, where a few $CaCO_3$ particles and fibres agglomerates were observed. (The colour of the polyester particles should blend in with the colour of the epoxy matrix, thus making difficult to identify them.) The glass
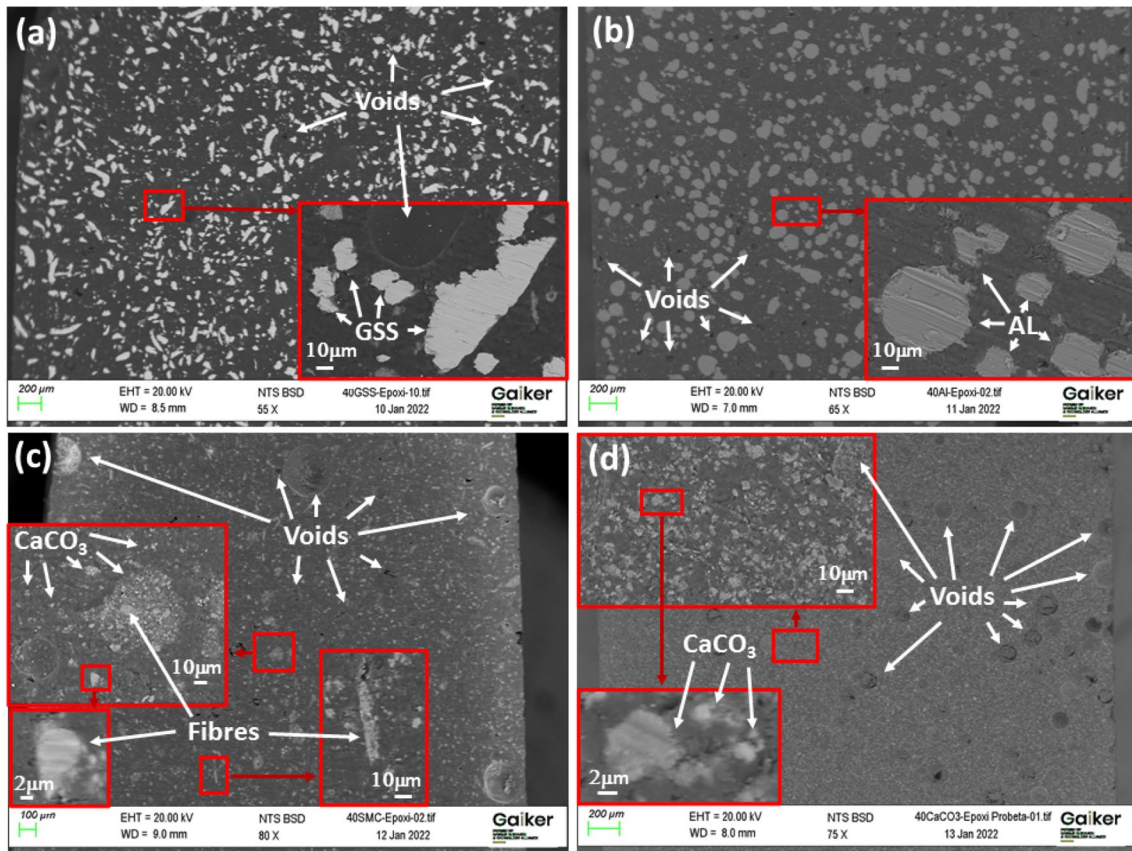
Fig. 8 SEM micrographs of 40GSS/4GA/EP (**a**), 40AL/4GA/EP (**b**), 40SMC/4GA/EP (**c**) and 40CaCO$_3$/4GA/EP (**d**) at different magnifications

Table 5 Cost per kilogram of eight blends

Filler content (wt%)	10 (€/kg)	20 (€/kg)	30 (€/kg)	40 (€/kg)
AL/EP	9.92	9.54	9.16	8.78
GSS/EP	9.27	8.24	7.21	6.18
CaCO$_3$/EP	9.34	8.38	7.42	6.46
SMC/EP	9.27	8.24	7.21	6.18

fibres (with an elongated or elliptical shape and a diameter of approximately 10 mm) were also homogeneously distributed in the matrix, and no gaps between these filaments and the matrix were observed, nor aluminium and CaCO$_3$ composites were noticed in the GSS. This confirmed that

a good matrix–filler interface existed, which indicated that the interaction between components was satisfactory.

Cost analysis and PMC selection

The cost per kilo of each PMC is shown in Table 5. As can be seen, the cheapest compounds correspond to 40GSS/4GA/EP and 40SMC/4GA/EP. It is obvious that the more filler is added the cheaper the blend; moreover, this effect is boosted when the filler is costless. This saving is clearly reflected in the cost of the raw material required for the manufacturing of four different mould sizes (Table 6). It can be observed that the larger the mould, the greater the savings, which is somewhat obvious, so if 40GSS/4GA/EP-40SMC/4GA/EP were selected for the mould manufacturing instead of

Table 6 Cost of raw material to manufacture 40GSS/4GA/EP and 40GSS/4GA/EP-40SMC/4GA/EP moulds

Type of mould	Small (60 dm^3)	Medium (500 dm^3)	Large (1700 dm^3)	Very large (4000 dm^3)
40AL/4GA/EP	750 €	6251 €	21,254 €	50,010 €
40GSS/4GA/EP-40SMC/4GA/EP	540 €	4498 €	15,293 €	35,982 €

40AL/4GA/EP, then a reduction in expenditure of €14,028 could be obtained.

Table 7 is used to select the most advantageous PMC for manufacturing the thermally conductive zone of medium-to-large moulds. This valuation matrix selected 40GSS/4GA/EP and 40AL/4GA/EP as the first and second most favourable compounds, respectively. The greatest advantages of 40GSS/4GA/EP were its low cost and its hardness, with an improvement of 29.6% and 8.5%, respectively, compared to 40AL/4GA/EP. On the contrary, for all other properties it was exceeded by 40AL/4GA/EP.

Properties such as density, hardness and compressive strength are considered of little importance, since density only affects mould manageability and hardness and compressive strength is of even less relevance, because a silicone release cover is placed between the part and the mould. Tensile strength and flexural modulus are considered of moderate importance, because the weaker the mechanical properties of the materials, the greater the amount of material that has to be used to compensate for that weakness. Thermal conductivity is considered very important since it affects the dimensional quality of parts (Tatara 2017). The cost of the material is considered extremely important, because the cost of the mould is one of the issues that must be addressed, to reduce the cost per part in small batch production.

It should be noted that the weighting factors such as density and cost may vary depending on the size of the mould. For instance, these weightings may fall to 1 and 4, respectively, for small moulds, since the mould weight loses relevance, and the mould fabrication labour costs gain relevance when compared to the raw material costs.

Table 8 is used to choose the most favourable PMC for manufacturing the thermal barrier of medium-to-large moulds. This valuation matrix chose 40SMC/4GA/EP and 30SMC/4GA/EP as the first and second most advantageous composites, respectively. The most remarkable benefits of 40SMC/4GA/EP were its low thermal conductivity and density, with an improvement of 30.1% and 9.0%, respectively, compared to 40CaCO$_3$/4GA/EP. On the contrary, for tensile strength and hardness it was exceeded by 40CaCO$_3$/4GA/EP. Unlike Table 7, Table 8 valuation matrix considers the thermal conductivity attribute extremely important because the thermal insulation is a characteristic of the mould that needs to be maximized to reduce the heat dissipation to the ambient.

Mould performance

Pressures below 0.2 MPa led to consolidation of the piece before proper compaction of the layers. The required pressure depends on the quantity and nature of fillers, additives and reinforcements, as well as moulding temperature, part thickness, part complexity, compression speed, etc. (Pizzi and Ibeh 2014). As a result, several moulding defects occurred: warpage of the part, weld lines, cavities within the part and non-merging of laminas (Fig. 9). On the contrary, when the pressure exceeded 0.9 MPa, considerable burrs began to appear on the moulded parts, because the clearance of the mould closure (1.5 mm) was considerably greater than the typical gap of 0.06–0.10 mm designed for steel production moulds (Cybulski 2009). The mould was designed with this clearance to avoid any risk of friction

Table 7 Valuation matrix for the PMC selection (thermally conductive zone)

| Property	Density (gr/cm^3)		Tensile strength (MPa)		Flexural modulus (MPa)		Compression strength (MPa)		Hardness		Thermal conductivity (w/mk)		Cost (€/kg)		Valuation
	2	A	3	B	3	C	2	D	2	E	4	F	5	G	2(1-A)+3B+3C+2D+2E+4F+5(1-G)
Specimen ID	Abs	W	Abs	W	Abs	W	Abs	W	Abs	W	Abs	W	Abs	W	
10GSS/4GA/EP	1.19	0.71	56.10	1.00	2855	0.75	78.00	0.82	40	0.86	0.24	0.48	9.27	0.93	11.44
20GSS/4GA/EP	1.33	0.80	46.70	0.83	3145	0.83	84.20	0.89	41	0.88	0.29	0.58	8.24	0.83	12.08
30GSS/4GA/EP	1.44	0.87	46.60	0.83	3279	0.86	93.30	0.98	44	0.95	0.30	0.60	7.21	0.73	12.97
40GSS/4GA/EP	1.66	1.00	44.00	0.78	3654	0.96	94.90	1.00	47	1.00	0.43	0.86	6.18	0.62	14.56
10AL/4GA/EP	1.17	0.70	53.60	0.96	3280	0.86	84.60	0.89	37	0.80	0.24	0.48	9.92	1.00	11.35
20AL/4GA/EP	1.24	0.75	47.60	0.85	3460	0.91	90.80	0.96	39	0.85	0.30	0.60	9.54	0.96	11.98
30AL/4GA/EP	1.31	0.79	45.00	0.80	3650	0.96	92.10	0.97	41	0.88	0.37	0.74	9.16	0.92	12.74
40AL/4GA/EP	1.42	0.86	40.80	0.73	3800	1.00	93.30	0.98	43	0.92	0.50	1.00	8.78	0.89	13.85

Abs. Absolute value

W. Weighted value

Table 8 Valuation matrix for the PMC selection (thermal barrier)

Property	Density (gr/cm³)		Tensile strength (MPa)		Flexural modulus (MPa)		Compression strength (MPa)		Hardness		Thermal conductivity (w/mk)		Cost (€/kg)		Valuation
	2	A	3	B	3	C	1	D	1	E	5	F	5	G	2(1-A)+3B+3C+D+E+5(1-F)+5(1-G)
Specimen ID	Abs	W	Abs	W	Abs	W	Abs	W	Abs	W	Abs	W	Abs	W	
10SMC/4GA/EP	1.02	0.79	31.6	0.84	2889	0.85	49.1	0.78	37	0.86	0.18	0.68	9.27	0.99	8.75
20SMC/4GA/EP	1.08	0.84	29.9	0.80	3169	0.93	60.2	0.95	38	0.88	0.19	0.73	8.24	0.88	9.28
30SMC/4GA/EP	1.09	0.84	20.4	0.54	3219	0.94	61.9	0.98	40	0.93	0.19	0.75	7.21	0.77	9.10
40SMC/4GA/EP	1.17	0.91	19.2	0.51	3369	0.99	63.1	1.00	41	0.95	0.18	0.70	6.18	0.66	9.83
10CaCO$_3$/4GA/EP	1.09	0.84	37.5	1.00	2780	0.82	52.1	0.83	36	0.84	0.19	0.74	9.34	1.00	8.71
20CaCO$_3$/4GA/EP	1.11	0.86	26.8	0.71	2950	0.87	57.9	0.92	41	0.95	0.23	0.89	8.38	0.90	7.98
30CaCO$_3$/4GA/EP	1.22	0.94	24.5	0.65	3410	1.00	61.1	0.97	43	1.00	0.23	0.88	7.42	0.79	8.68
40CaCO$_3$/4GA/EP	1.29	1.00	24.8	0.66	3366	0.99	60.8	0.96	43	1.00	0.26	1.00	6.46	0.69	8.45

Abs. Absolute value

W. Weighted value
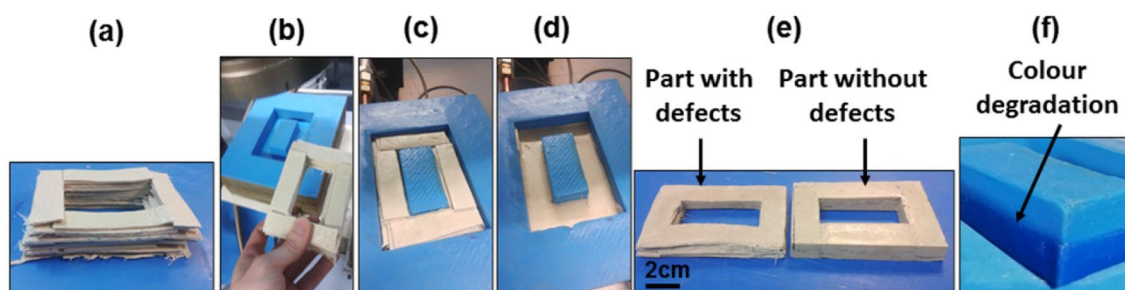
Fig. 9 Moulding tests. (**a**) SMC stack-up. (**b**) Manual introduction of the stack-up. (**c**) SMC stack-up before moulding. (**d**) SMC stack-up after moulding. (**e**) Moulded parts. (**f**) Colour degradation of the silicone rubber cover

between the female and male moulds during closing, due to a thermal expansion of the silicone rubber and a relatively low-dimensional accuracy of the master models manufactured by FDM printing.

A mould with shorter closure distance could be redesigned and re-manufactured; however, there was no advantage in increasing the pressure above 0.9 MPa to mould these thick parts, as there was no textured finish, or complex surface to be copied such as ribs or bosses, which certainly require more pressure depending on the degree of their complexity (Tatara 2017).

So, considering the typical moulding pressures with steel moulds of 10-15 MPa (Tatara 2017) and the recorded pressure (0.2 MPa), it can be affirmed that the pressure needed to mould these parts properly was 50 times less than the standard moulding pressure. Moreover, according to Duranik et al. (2013) this pressure may drop by 60–70%

if the charge is preheated, for instance, with microwaves or radio frequencies (advantageous in thick parts, because heating is internalized).

For instance, a 0.44m² (projected area) part moulded with a pressure of 15 MPa will require a 660 tons press, whereas moulding with a pressure of 0.2 MPa, will only demand a 9 tons press. As a result, low tonnage and consumption presses, such as a cost-effective pneumatic press of 9 tons could be used, which is a practical solution using the standard 6.9 bar plant air pressure. So, considering that typical compression presses vary between 100 and 5000 tons, this low-pressure technique could be used for the manufacture of parts larger than the standard technique, i.e. larger than 3 m² (Hollaway 1994).

This pressure reduction to 0.2 MPa and 0.9 MPa was possible due to a methodology where the moulding material is placed on more or less 80% of the moulding surface, rather

than the typical SMC placement percentages (< 40%) (Kluge et al. 2015). This strategy also minimizes the risk of silicone cover breakage, due to an excessive flow of the SMC within the mould and the relatively low tensile strength of the silicone rubber (Su et al. 2020). Furthermore, the degree of anisotropy of the moulded part is reduced with increased mould coverage, which affects to shrinkage, residual stresses and warping (Tatara 2017). Nevertheless, when the moulding surface is occupied in a percentage close to 100%, air entrapment leads to voids and even delamination of the moulded part (Ma et al. 2017).

Regarding the developed demoulding system, the 4-mm-thick silicone rubber cover was removed (with some effort) from the female mould without any complex and expensive demoulding mechanism, despite the length of the inner core. Thinner cover (2 mm thickness) led to cover tearing after moulding 23 parts, whereas the thicker cover extended its service life up to 100 mouldings with some loss of elasticity and colour degradation (Fig. 9), which could probably lead to a breakage of the cover after certain mouldings. It seems that the polyester SMC (due to its styrene content) would affect negatively to the silicone rubber (Novotema; Williams et al. 1996).

Therefore, the thickness of the silicone rubber cover possesses the greatest relevance, as it is subjected to a quite high tear force during the extraction and the tear strength of the silicone rubber decreases drastically with the temperature and its loss of elasticity (Su et al. 2020). So, if more than a hundred parts are required to be manufactured, it would probably be necessary to re-manufacture silicone covers; therefore, it must register the weight of each silicone casting of the first manufactured cover to ensure repeatability of manufactured covers.

Once the silicone cover with the part is extracted from the mould, the moulded part can be easily removed from these mould release shells, because these covers avoid any mechanical adhesion of the SMC to some porosities that emerge on the surface of the mould (Fig. 10). This issue was also encountered by other researchers (Pontes et al. 2010; Goncalves et al. 2007) where a silicon-based release agent was applied to the moulding surface, without fully resolving the demoulding problems. In addition, chemical adhesion between the SMC and the mould occurred when the surface of the mould reached a temperature close to the Tg of the resin. If for extraordinary reasons the mould might be overheated, then the use of these covers avoids this problem.

Mould energy consumption

Figure 11 shows the registered temperatures in two locations (over eight hours) of the moulds both with and without thermal barrier. The thermocouple located at the oil inlet of both
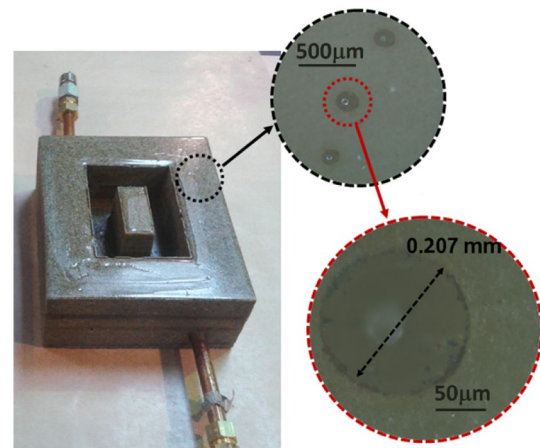
Fig. 10 Surface porosity observations of the mould with an optical microscope

moulds registered sawtooth temperature variations between approximately 130 °C and 110 °C over time.

The thermocouple placed on the mould with the thermal barrier recorded data to indicate that the switch-on and the switch-off periods lasted 3.8 min and 24.7 min (green line), respectively, whereas the thermocouple located at its none thermally isolated counterpart indicated that the switch-on and the switch-off periods lasted 4.1 min and 20.6 min (blue line), respectively.

Therefore, the number of times that the resistor switched on, to keep the mould with the thermal barrier at approximately 120°C, was less than for the mould with no thermal isolation. As a result, the oil heating machine resistor connected to the mould with no thermal barrier was, over one working day, active for a longer period, resulting in higher energy consumption.

Somehow, this effect is supported by the fact that the temperature of the thermocouple located at the (40GSS/4GA/EP—40SMC/4GA/EP) mould wall (purple line) registered lower temperatures than the 40GSS/4GA/EP mould (red line). It means that the energy in the form of heat, is kept in the volume that encloses the thermal barrier, specifically in that volume made with 40GSS/4GA/EP. As a result, heat dissipation is lower from the mould to the ambient atmosphere and consequently, less consumption of electricity is required.

The energy consumption of the mould with the thermal barrier compared to its counterpart with no thermal isolation is shown by the light blue line and the orange line, respectively, in Fig. 11. The electricity consumed in a working day (considering a steady-state regime) for the none thermally isolated mould reached 36.9 MJ, whereas the thermally isolated mould consumed 29.1 MJ, implying a reduction in energy consumption of 27%.

Fig. 11 Registered temperatures and energy consumption of 40GSS/4GA/EP and 40GSS/4GA/EP—40SMC/4GA/EP moulds
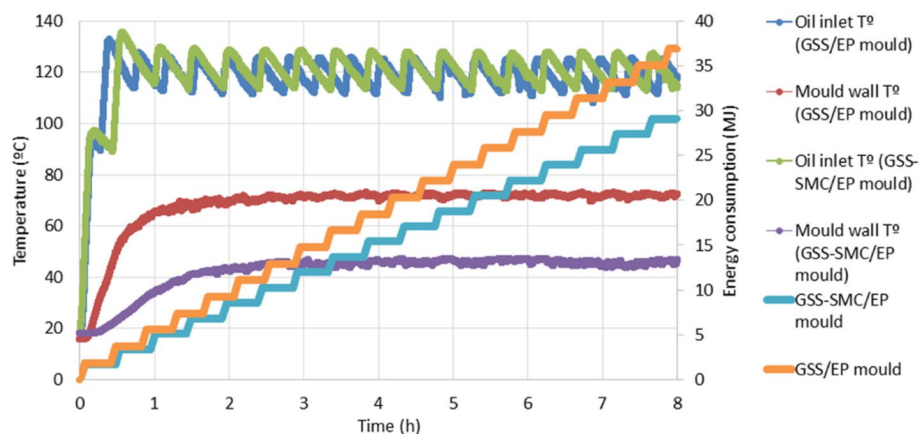
Conclusions

In this study, SMC and GSS waste has been recovered and used to make a cost-effective hot-press compression mould for energy efficient SMC moulding. Mechanical, thermal and physical properties of the created PMCs have been studied through tensile, flexural, compressive, DSC, hardness and density tests, for eventual verification of its suitability in mould manufacturing through monitored moulding tests. Based on the results discussed in this research, the following conclusions can be drawn.

Metal and GFRP machining are one of the most widely used methods for part post-processing and tool manufacturing, so in view of the results obtained and the large availability of these residues, GSS and SMC could be used as a source of raw material and as a substitute for commercial aluminium and $CaCO_3$ powder for manufacturing moulds, which is an effective approach to recover these wastes and thereby prevent the depletion of natural resources.

An effective solution to avoid the sedimentation of high-density fillers in thermoset matrices using an additive with anti-settling properties is proposed. This solution is simpler than the use of accelerators or a non-commercially available anti-settling device that requires a very precise time measurement.

40GSS/4GA/EP and 40SMC/4GA/EP compounds were the most advantageous for mould making. On the one hand, 40GSS/4GA/EP has 8.5%, more hardness, and it costs 29.6% less than its counterpart in aluminium (40AL/4GA/EP) that leads to more economical moulds, which is clearly advantageous for short production batches. On the other hand, 40SMC/4GA/EP is the most beneficial PMC to implement a cost-effective thermal barrier in the mould, because its thermal conductivity and cost per kilo is 30.1% and 4.3%, respectively, lower than $40CaCO_3$/4GA/EP.

The utility of the manufactured mould has been empirically tested for hot-press compression moulding, proving that the developed PMCs can withstand the moulding conditions. Furthermore, the method of placing the SMC covering over a large part of the moulding surface prevents the breakage of the silicone rubber cover and enables moulding at lower pressures, thus expanding the scope of the technique to larger parts and the use of presses of lower tonnage and consumption.

The use of silicone rubber covers located at moulding surfaces is a useful and efficient tool to provide a release of moulded parts even with large inner cores. Furthermore, it contributes to avoid the use of complex and expensive demoulding mechanisms that considerably increase the cost of the mould, making it more appropriate for short production batches.

The mould with the thermal barrier required 27% less electricity than the mould without the thermal barrier during an eight-hour moulding routine, savings that were achieved thanks to an external non-conductive thermal wall built in 40SMC/4GA/EP. Moreover, this economically competitive mould showed a cost saving of 39% in comparison with the 40AL/4GA/EP mould.

Declarations

References

Barone MR, Caulk DA (1980) Compression molding: nonuniform cavity surface temperature and cycle time. In: Proceedings of

the First International Conference on reactive processing of polymers. Pittsburgh. PA

Barone MR, Caulk DA (1979) The effect of deformation and thermoset cure on heat conduction in a chopped-fiber reinforced polyester during compression moulding. Int J Heat Mass Transf 22(7):1021–1032

Bernard A, Fischer A (2002) New trends in rapid product development. CIRP Ann-Manuf Techn 51:635–652

Bhagyashekar MS, Rao RMVGK (2010) Characterization of mechanical behavior of metallic and non-metallic particulate filled epoxy matrix composites. J Reinf Plast Comp 29(1):30–42

Bhagyashekar MS, Kavaitha R, Rao RMVGK (2009) Studies on rheological and physical properties of metallic and non-metallic particulate filled epoxy composites. J Reinf Plast Compos 28:2869–2878

Burmistrov IN, Shatrova NV, Mostovoy AS, Mazov IN, Kuznetsov DV, Panova LG, Gorokhovsky AV, Yudin AG (2014) Mechanical properties of (surface-modified potassium polytitanate small additives)/epoxy composite materials. Polym Eng Sci 54:2866–2871

Callister WD (1999) Materials science and engineering: an introduction. Wiley, New York

Chiu SH, Wu CL, Gan SY, Chen KT, Wang YM (2015) Thermal and mechanical properties of copper/photopolymer composite. Rapid Prototyp J 22(9):684–690

Chung S, Im YG, Kim H, Park S, Jeong H (2005) Evaluation for micro scale structures fabricated using epoxy-aluminum particle composite and its application. J Mater Process Technol 160:168–173

Cybulski E (2009) Plastic conversion processes. CRC Press, Boca Raton

da Costa CE, Zapata WC, Parucker ML (2003) Characterization of casting iron powder from recycled swarf. J Mater Process Technol 143–144:138–143

Davis BA, Gramann PJ, Osswald TA, Rios AC (2003) Compression molding. Hanser Gardner Publications, Cincinnati

de Carvalho A, Fagali A, Leite J (2016) Mechanical and dimensional characterisation of polypropylene injection moulded parts in epoxy resin/aluminium inserts for rapid tooling. Int J Mater Prod Tec 52:37–52

Duranik T, Ruzbarsky J, Stopper M (2013) Influence on the productivity of modern thermoset preheating in the compression molding technology. Adv Mat Res 717:47–78

Fettea M, Sanderb P, Wulfsbergc J, Zierkd H, Herrmanne A, Stoessf N (2015) Optimized and cost-efficient compression moulds manufactured by selective laser melting for the production of thermoset fibre reinforced plastic aircraft components. Proc CIRP 35:25–30

Flores I, Kretzschmar N, Azman AH, Chekurov S, Pedersen DB, Chaudhuri A (2020) Implications of lattice structures on economics and productivity of metal powder bed fusion. Addit Manuf 31:100947

Fu J, Shi L, Zhang D, Zhong Q, Chen Y (2010) Effect of nanoparticles on the performance of thermally conductive epoxy adhesives. Polym Eng Sci 50:1809–1819

Garcia D, Vegas I, Cacho I (2014) Mechanical recycling of GFRP waste as short-fiber reinforcements in microconcrete. Constr Build Mater 64:293–300

Goncalves MV, Salmoria GV, Ahrens CH, Pouzada AS (2007) Study of tribological properties of moulds obtained by stereolithography. Virtual Phys Prototyp 2:29–36

Gope PC, Singh VK (2011) Effect of filler addition and strain rate on the compressive strength of silica styrene-butadiene rubber-filled epoxy composites. Polym Eng Sci 51:1130–1136

Gutowski TG, Allwood JM, Herrmann C, Sahni S (2013) A global assessment of manufacturing: economic development, energy use, carbon emissions, and the potential for energy efficiency and materials recycling. Annu Rev Environ Resour 38:81–106

Hollaway LC (1994) Handbook of polymer composites for engineers. Elsevier, Amsterdam

Jensen JP, Skelton K (2018) Wind turbine blade recycling: experiences, challenges and possibilities in a circular economy. Renew Sust Energ Rev 97:165–176

Khorasani AM, Gibson I, Veetil JK, Ghasemi AH (2020) A review of technological improvements in laser-based powder bed fusion of metal printers. Int J Adv Manuf Tech 108:191–209

Khushairi MTM, Sharif S, Ani JSM (2015) Evaluation of mechanical properties of filled epoxy composite for improving mould performance – A review. Appl Mech Mater 735:13–18

Khushairi MTM, Sharif S, Jamaludin KR, Mohruni AS (2017) Effects of metal fillers on properties of epoxy for rapid tooling inserts. IJASEIT 7(4):1155–1161

Kluge NEJ, Lundström TS, Westerberg LG, Olofsson K (2015) Compression moulding of sheet moulding compound: modelling with computational fluid dynamics and validation. J Reinf Plast Compos 34:479–492

Kuo CC, Li MR (2017) Development of sheet metal forming dies with excellent mechanical properties using additive manufacturing and rapid tooling technologies. Int J Adv Manuf Tech 90:21–25

Lechtenböhmer S, Nilsson LJ, Ahman M, Schneider C (2016) Decarbonising the energy intensive basic materials industry through electrification e Implications for future EU electricity demand. Energy 115:1623–1631

Leite JL, Salmoria GV, Ahrens CH, Pouzada AS (2013) Characterization of epoxy/steel fibres composites for hybrid injection moulds. Mater Sci Forum 730:277

Liu Y, Dong H, Lohse N, Petrovic S (2016) A multi-objective genetic algorithm for optimisation of energy consumption and shop floor production performance. Int J Prod Econ 179:259–272

Lokensgard E (2010) Industrial plastics: theory and applications. Delmar Cengage Learning, New York

Ma S, Gibson I, Balaji G, Hu QJ (2007) Development of epoxy matrix composites for rapid tooling applications. J Mater Process Technol 192–193:75–82

Ma Y, Centea T, Nutt SR (2017) Defect reduction strategies for the manufacture of contoured laminates using vacuum BAG-only prepregs. Polym Compos 38(9):2016–2025

Mahshid R, Hansen HN, Højbjerre KL (2016) Strength analysis and modeling of cellular lattice structures manufactured using selective laser melting for tooling applications. Mater Des 104:276–283

Meng LL, Zhang CY, Shao XY et al (2019) MILP models for energy-aware flexible job shop scheduling problem. J Clean Prod 210:710–723

Modarresifar F, Bingham PA, Jubb GA (2016) Thermal conductivity of refractory glass fibres: A study of materials, standards and test methods. J Therm Anal Calorim 125:35–44

Mostovoi AS, Ledenev AN, Panova LG (2017) Modification of epoxy matrix by whiskers of potassium polytitanate. Inorg Mater 8:755–758

Nakamura K (2004) NTN Technical Review No. 71. p. 80

Nayak S, Satapathy A, Mantry S (2020) Processing and wear response study of glass-polyester composites with waste marble dust as particulate filler. Polym Compos 41:2263–2273

Thermal Analysis Application No. UC 226, Application published in Mettler Toledo Thermal Analysis UserCom 22, 2010

Nóvoa P, Ribeiro MCS, Ferreira AJM, Marques ATM (2004) Mechanical characterization of lightweight polymer mortar modified with cork granulates. Compos Sci Technol 64:2197–2205

Novotema. Elastomer types and chemical compatibility. https://en.novotema.com/assets/uploads/brochures/N1021A_Novotema_Elastomer_Chemical_Compatibility_Brochure_EN.pdf. Accessed 20 May 2021

Osugi R, Takagi H, Liu K, Gennai Y (2009) Thermal conductivity behavior of natural fiber-reinforced composites. In: Asian Pacific Conference for Materials and Mechanics, Yokohama, Japan

Pan C, Han Y, Lu J (2020) Design and optimization of lattice structures: a review. Appl Sci 10:6374

Pizzi A, Ibeh CC (2014) Handbook of thermoset plastics. Elsevier, Amsterdam

Pontes AJ, Queiros MP, Martinho PG, Bartolo PJ, Pouzada AS (2010) Experimental assessment of hybrid mould performance. Int J Adv Manuf Tech 50:441–448

Reis JML, Jurumenha MAG (2013) Investigation on the effects of polymer impregnated aggregate on polymer mortars properties. Mater Struct 46:1383–1388

Ribeiro MCS, Meixedo JP, Fiúza A, Dinis ML, Castro ACM, Silva FG, Costa C, Ferreira F, Alvim MR (2011) Mechanical behaviour analysis of polyester polymer mortars modified with recycled GFRP waste materials. Int J Mech Mechatron Eng 5(3):707–713

Ribeiro MCS, Fiúza A, Castro ACM, Silva FG (2013) Mix design process of polyester polymer mortars modified with recycled GFRP waste materials. Compos Struct 105:300–310

Ribeiro MCS, Meixedo JP, Fiúza A, Dinis ML, Castro ACM, Silva FG, Costa C, Ferreira F, Alvim MR (2016) Recycling approach towards sustainability advance of composite materials industry. Recycling 1(1):178–193

Salido M, Escamilla J, Barber F, Giret A (2017) Rescheduling in job-shop problems for sustainable manufacturing systems. J Clean Prod 162:121–132

San-Jose JT, Sancibrian R, Blanco JM, Rojo E, Marcos I, Larrauri MI (2015) Teaching students how to solve complex engineering problems by using decision making approaches: value analysis. In: 9th International technology, education and development conference, Madrid. Spain

Seetharam PG, Bhuvaneswari C, Vidhya S, Vishnu PM (2017) Studies on properties of concrete replacing GGBS, steel slag and slate. IJERT 6:387–393

Sheehan E, Braun AT, Kuhlmann T, Sauer A (2016) Improving material efficiency for ultra-efficient factories in closed-loop value networks. Procedia CIRP 40:455–462

Shuaib NA, Mativenga PT (2016) Energy demand in mechanical recycling of glass fibre reinforced thermoset plastic composites. J Clean Prod 120:198–206

Shukla KA (2013) Application of CNC waste with recycled aggregate in concrete mix. IJERT 3(4):1026–1031

Su J, Du B, Jin Li, Li Z (2020) Electrical tree degradation in high-voltage cable insulation: progress and challenges. High Volt 5(4):353–364

Takagi H, Miyazaki T, Tamatani J (2012) Recycling technology for grinding swarf: application to iron powder for disposable body warmer. Appl Mech Mater 121–126:1535–1539

Tatara RA (2017) Applied plastics engineering handbook: processing, materials, and applications. Elsevier, Amsterdam

Tiwari S, Gehlot CL, Srivastava D (2020) Epoxy/Fly ash from Indian soil Chulha/nano $CaCO_3$ nanocomposite: Studies on mechanical and thermal properties. Polym Compos 41:3237–3249

Tomori T, Melkote S, Konis M (2004) Injection mold performance of machined ceramic filled epoxy tooling boards. J Mater Process Technol 145:126–133

Tuo J, Liu F, Liu P, Zhang H, Cai W (2018) Energy efficiency evaluation for machining systems through virtual Part. Energy 159:172–183

Vakili MH, Dehaghani HE, Haghshenas M (2011) Crystallization and thermal conductivity of $CaCO_3$ nanoparticle filled polypropylene. J Macromol Sci Phys 8:1637–1645

Vasconcelos PV, Lino FJ, Baptista AM, Neto RJL (2006) Tribological behavior of epoxy based composites for rapid tooling. Wear 260:30–39

Williams C, Summerscales J, Grove S (1996) Resin infusion under flexible tooling (RIFT): a review. Compos Part A-Appl S 27(7):517–524

Winter M, Li W, Kara S, Herrmann C (2014) Determining optimal process parameters to increase the eco-efficiency of grinding processes. J Clean Prod 66:644–654

Xu W, Shao L, Yao B, Zhou Z, Pham D (2016) Perception data-driven optimization of manufacturing equipment service scheduling in sustainable manufacturing. J Manuf Syst 41:86–101

Yan J, Li L, Zhao F, Zhang F, Zhao Q (2016) A multi-level optimization approach for energy-efficient flexible flow shop scheduling. J Clean Prod 13:1543–1552

Yin J, Meng X, Bian B, Zhang J, Yin Y (2020) Effect of particle type and its surface characteristics on the mechanical properties of particle-filled polymer composite for precision machine tools. Polym Compos 41:972–981

Yusof M, Afifi AM, Razali NT, Sawawi M, Karim ARA (2018) Calcium carbonate from clam shell as a thermal conductor in particulate filled polymer matrix composites. Int J Eng Technol 7:101–105

Publisher's Note Springer Nature remains neutral with regard to jurisdictional claims in published maps and institutional affiliations.